Journal of Power Sources 195 (2010) 2174–2181

Contents lists available at ScienceDirect

Journal of Power Sources

journal homepage: www.elsevier.com/locate/jpowsour

Performances of $LnBaCo_2O_{5+x}$–$Ce_{0.8}Sm_{0.2}O_{1.9}$ composite cathodes for intermediate-temperature solid oxide fuel cells

Qingjun Zhou, Fang Wang, Yu Shen, Tianmin He*

National Laboratory of Superhard Materials, and College of Physics, Jilin University, 2519 Jiefang Road, Changchun 130012, Jilin, PR China

ARTICLE INFO

Article history:
Received 2 September 2009
Received in revised form 20 October 2009
Accepted 20 October 2009
Available online 30 October 2009

Keywords:
Solid oxide fuel cell
Composite cathode
Cobaltite
Double perovskite
Electrochemical performance
Thermal expansion

ABSTRACT

Double-perovskite oxides, $LnBaCo_2O_{5+x}$ (LnBCO) (Ln = Pr, Nd, Sm, and Gd), are prepared using a solid-state reaction as cathodes for intermediate-temperature solid oxide fuel cells (IT-SOFCs). The performances of LnBCO–$Ce_{0.8}Sm_{0.2}O_{1.9}$ (SDC) composite cathodes were investigated for IT-SOFCs on $La_{0.9}Sr_{0.1}Ga_{0.8}Mg_{0.2}O_{3-\delta}$ (LSGM) electrolyte. The thermal expansion coefficient can be effectively reduced in the case of the composite cathodes. No chemical reactions between LnBCO cathodes and SDC electrolyte, and LnBCO and LSGM are found. The electrochemical performances of LnBCO cathodes and LnBCO–SDC composite cathodes decrease with decreasing Ln^{3+} ionic radii, which is closely related to the decrease of the electrical conductivity and fast oxygen diffusion property. The area specific resistances of the LnBCO cathodes and LnBCO–SDC composite cathodes on LSGM electrolyte are all lower than 0.13 Ω cm^2 and 0.15 Ω cm^2 at 700 °C, respectively. The maximum power densities of single-cell consisted of LnBCO–SDC composite cathodes, LSGM electrolyte, and Ni–SDC anode achieve 758–608 mW cm^{-2} at 800 °C with the change from Ln = Pr to Gd, respectively. These results indicate that LnBCO–SDC composite oxides are candidates as a promising cathode material for IT-SOFCs.

1. Introduction

Solid oxide fuel cells (SOFCs) are all-solid electrochemical devices that convert chemical energy directly into electrical energy with high efficiency and low emission of pollutants [1]. Traditional SOFC using yttria stabilized zirconia (YSZ) as electrolyte operates at high temperature of about 1000 °C, which can result in a series of problems such as the electrode sintering, interface reaction between cell components, and high material and manufacture costs. Therefore, there is great interest in reducing the operation temperature of SOFCs to the intermediate-temperature range of 600–800 °C. Developing intermediate-temperature solid oxide fuel cells (IT-SOFCs) not only can significantly reduce the costs of SOFCs, but also can effectively extend the choice of materials, thus improves the reliability and the service lifetime of SOFCs. However, the cathode overpotential and interfacial resistance will increase rapidly as the operating temperature of SOFCs is decreased. Therefore, the development of high performance cathodes with low polarization losses and high stability has become increasingly critical for the development of IT-SOFCs.

Perovskite oxides, particularly of the mixed ionic and electronic conductors (MIECs), are the most commonly used cathode materials for IT-SOFCs due to their high-electrocatalytic activity for the oxygen-reduction reaction [2]. Recently, double-perovskite oxides, $LnBaCo_2O_{5+x}$ (LnBCO) (Ln = La, Pr, Nd, Sm, Gd, and Y) have received increased attention due to their possible application on cathodes for IT-SOFCs [3–12]. These double-perovskite oxides with *112-type* structure in which the LnO and BaO layers alternate along the *c*-axis and oxygen vacancies are localized into LnO layers [13,14]. The distribution of vacancies in these oxides could greatly enhance oxygen transport properties. The existence of ordered oxygen-deficiency in double-perovskite oxides LnBCO (Ln represents a rare-earth element) has stimulated the research on magnetic properties. Most of the investigations of LnBCO materials have focused extensively on the structural, electrical and magnetic properties at low temperatures [13–20]. However, the high-temperature properties of these double-perovskite oxides LnBCO are still lacking. Therefore, the further research on the high-temperature properties is required. As a new family of cathode materials with double-perovskite structure, LnBCO cathodes with a single lanthanide-ion have been recently reported, such as PrBCO [21,22], NdBCO [23], SmBCO [24,25], GdBCO [26–28] and YBCO [29]. And these double-perovskite cathodes have showed good electrical conductivity and high-electrocatalytic activity for the oxygen-reduction reaction. However, these cathode materials have high thermal expansion coefficients (TECs) that are not compatible with those of intermediate-temperature electrolyte materials, for example, the TECs of LnBCO ranged from 24.3×10^{-6} K^{-1} to 15.8×10^{-6} K^{-1} in the temperature range of 80–900 °C in air with

* Corresponding author. Tel.: +86 431 88499039; fax: +86 431 88498000.
E-mail address: hly@mail.jlu.edu.cn (T. He).

0378-7753/$ – see front matter © 2009 Elsevier B.V. All rights reserved.
doi:10.1016/j.jpowsour.2009.10.062

the change from Ln = La to Y [8]. The thermal expansion incompatibility can cause thermal stress in the SOFC and thus results in its long-term stability performance deterioration. Therefore, it is important to improve the thermal expansion compatibility between the LnBCO cathodes and the electrolytes. In general, to lower the TEC of cathodes, one of the effective ways is to introduce electrolyte component into cathode to form composite cathodes [30].

In this study, we synthesized single phase LnBCO (Ln = Pr, Nd, Sm, and Gd) double-perovskite oxides by a solid-state reaction. A comparative study was carried out on the performance of LnBCO cathodes and LnBCO–$Ce_{0.8}Sm_{0.2}O_{1.9}$ (SDC) composite cathodes on $La_{0.9}Sr_{0.1}Ga_{0.8}Mg_{0.2}O_{3-\delta}$ (LSGM) electrolyte. The single-cell performances of LnBCO–SDC composite cathodes were also investigated for IT-SOFCs.

2. Experimental

2.1. Sample preparation

Double-perovskite oxides LnBCO were prepared using a conventional solid-state reaction [10]. Pr_6O_{11} (99.99%), Nd_2O_3 (99.9%), Sm_2O_3 (99.9%), Gd_2O_3 (99.99%), $BaCO_3$ (99%) and Co_2O_3 (99%) were used as starting materials. They were weighted in the stoichiometric proportions of LnBCO compositions. The mixtures were ground thoroughly with ethanol using an agate mortar and pestle for 1 h, then pressed into disks and calcined repeatedly at 1000 °C and 1050 °C in air with intermediate grindings, respectively. The calcined powders were ground again, pressed into disks and finally sintered at 1150 °C for 12 h in air. SDC, LSGM and NiO powders were prepared using a glycine-nitrite process as reported in previous paper [31]. Composite cathodes were prepared by mixing LnBCO powders with SDC powders in a weight ratio of 75:25. The mixtures were ground, pressed into cylinder samples with 6 mm in diameter and 6–8 mm in length for thermal expansion measurements. The samples were sintered at 1000 °C for 5 h.

2.2. Characterization

The phase composition of the synthesized powders and the phase reaction between cathode and electrolyte were identified using an X-ray diffractometer (XRD) (Rigaku-D-Max γA). The scans were performed in the 2θ range of 20–80° with an angle step of 0.02°, at room temperature. The reactivity of LnBCO with SDC and LSGM electrolytes was investigated through mixing and grinding the two powders in a weight ratio of 50:50 and sintered at 1000 °C for 5 h. The electrical conductivities were measured by the Van der Pauw method on sintered LnBCO samples of approximate dimensions ⌀13 mm × 1 mm in air. In this measurement, Ag paste was painted on edge of the disk samples on the symmetrical four corners to form current and voltage electrodes. The thermal expansion of the cylinder samples was measured using a horizontal dilatometer (Netzsch DIL 402C) over a temperature range of 30–1000 °C in air with a flowing rate of 60 ml min^{-1}, and a heating rate of 5 °C min^{-1}. Symmetrical cells with the configuration of electrode/LSGM/electrode were used for the impedance studies. Dense LSGM disks (⌀13 mm × 1 mm) were prepared by dry pressing and then were sintered at 1450 °C for 10 h in air. LnBCO cathodes and LnBCO–SDC composite cathodes were screen-printed onto the LSGM electrolytes and sintered at 950 °C for 2 h in air. Impedance spectra of the symmetrical cells were measured over the frequency range 0.1–10^5 Hz with the signal amplitude of 10 mV under open circuit, using an electrochemical system (CHI604C). A measurement temperature range of 700–800 °C was adopted in increments of 50 °C for all the samples. Microstructures of the symmetrical cell after testing were inspected using a scanning electron microscopy (SEM) (JEOL JSM-6480LV).

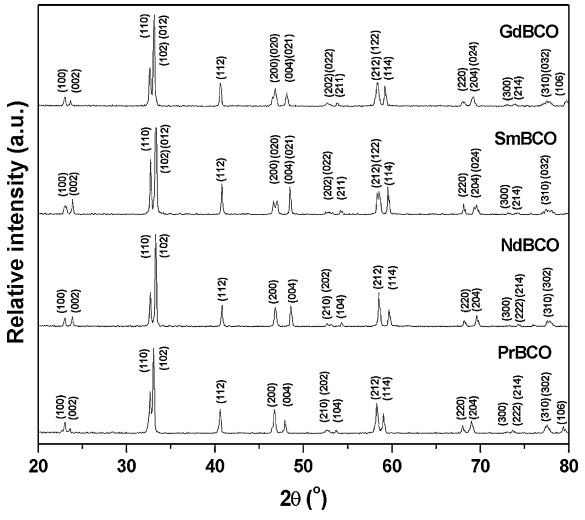

Fig. 1. XRD patterns of the LnBCO samples sintered at 1150 °C for 12 h in air.

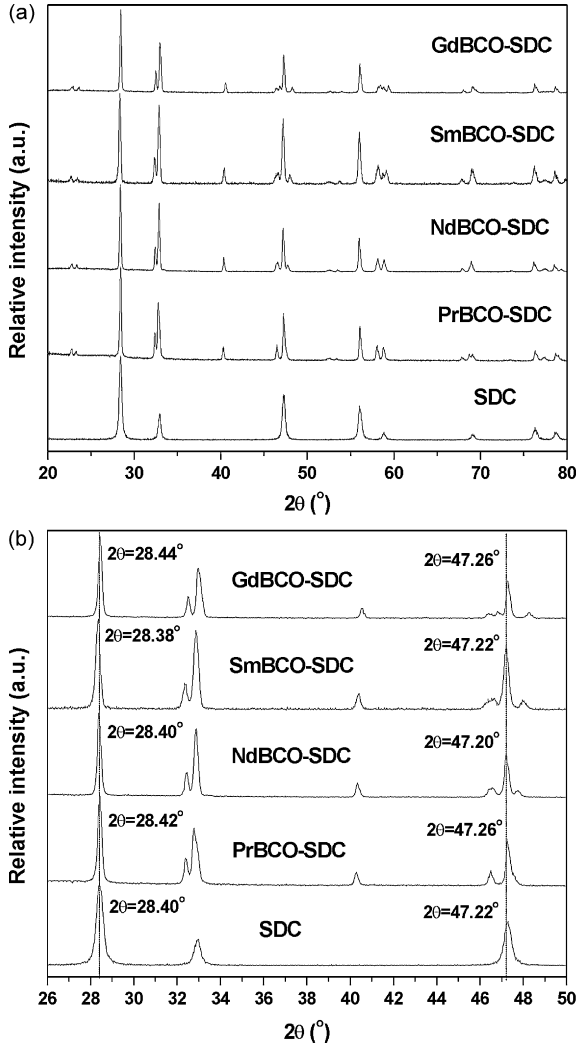

Fig. 2. (a) XRD patterns of SDC powders and LnBCO–SDC mixtures sintered at 1000 °C for 5 h, and (b) magnified XRD patterns of the peaks at the Miller indices of (1 1 1) and (2 2 0).

Electrolyte-supported fuel cells with the LSGM electrolyte were prepared using a screen printing method. LSGM were used as the electrolytes with a thickness of about 300 μm each. The anode was obtained from a mixture of NiO and SDC powders in a weight ratio of 65:35. For the fuel cells using LSGM as electrolyte, an SDC interlayer was introduced between the electrolyte and the anode and sintered at 1300 °C for 1 h. The anode and cathode were then sintered at 1250 °C for 4 h and 950 °C for 2 h in air to form the complete cells, respectively. The performance of the cells was measured under dry H_2 and ambient air in the temperature range 650–800 °C.

3. Results and discussion

3.1. XRD and chemical compatibility

Fig. 1 shows the XRD patterns (at room temperature) of the LnBCO samples sintered at 1150 °C for 12 h in air. It can be seen that all the oxides crystallize in a single phase double-perovskite after sintering at 1150 °C through intermediate grinding and calcining at 1000 °C and 1050 °C. The XRD patterns show the formation of a single phase double-perovskite without any additional diffraction peaks attributable to impurities detected. All the diffraction peaks of LnBCO samples can be indexed with an orthorhombic crystal structure. The results are in agreement with those reported by different groups [8,11,14,19]. The reaction between electrode and electrolyte is undesirable for the long-term stability of SOFCs. To assess the chemical compatibility between cathodes and electrolytes, the phase reaction of LnBCO cathodes with SDC and

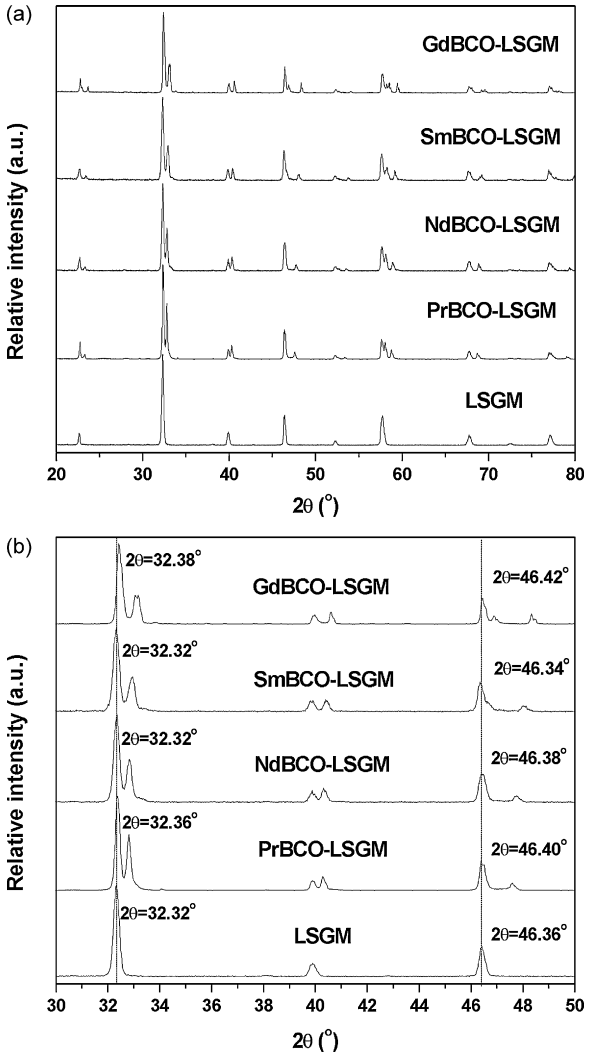

Fig. 3. (a) XRD patterns of LSGM powders and LnBCO–LSGM mixtures sintered at 1000 °C for 5 h, and (b) magnified XRD patterns of the peaks at the Miller indices of (1 2 1) and (2 0 2).

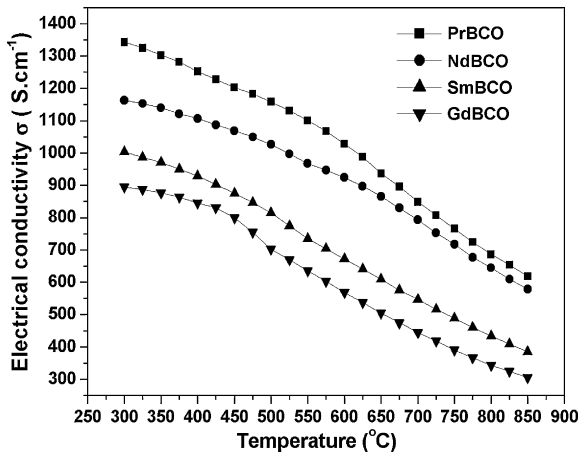

Fig. 4. Temperature dependence of the conductivity for LnBCO samples in air.

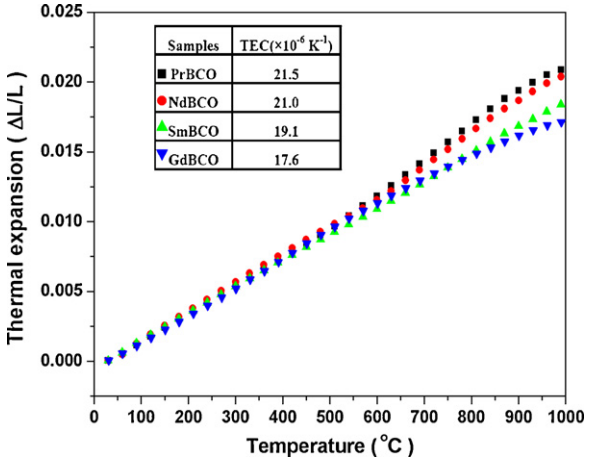

Fig. 5. Thermal expansion curves of the samples LnBCO in the temperature range 30–1000 °C in air.

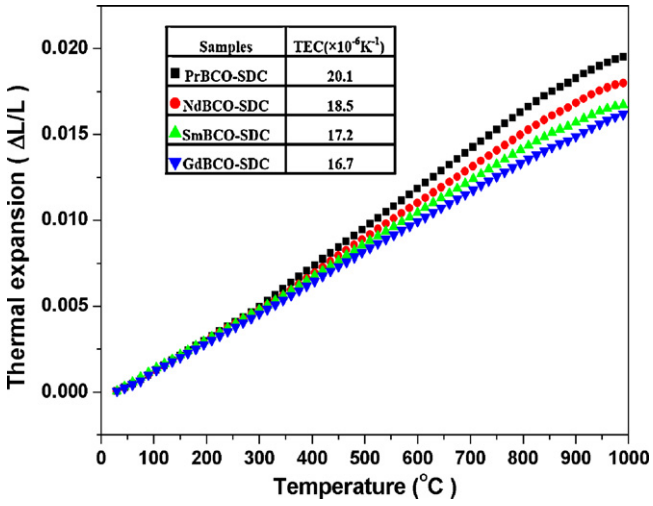

Fig. 6. Thermal expansion curves of the samples LnBCO–SDC in the temperature range 30–1000 °C in air.

LSGM electrolytes was examined with XRD analysis, respectively. Figs. 2(a) and 3(a) show the XRD patterns of SDC powders and LnBCO–SDC mixture, and LSGM powders and LnBCO–LSGM mixture sintered at 1000 °C for 5 h, respectively. The magnified XRD patterns for the diffraction angle range of 26° (30°) ≤ 2θ ≤ 50° are shown in Fig. 2(b) and 3(b), respectively. It can be seen from Figs. 2 and 3 that all the diffraction peaks can be identified with a physical mixture of LnBCO–SDC and LnBCO–LSGM phases, respectively. There are no additional peaks and obvious shift of XRD peaks in the patterns. The structures of LnBCO, SDC and LSGM oxides remain unchanged. No significant chemical reaction occurs between LnBCO and SDC, and LnBCO and LSGM electrolytes. This indicates that LnBCO oxides have a good chemical compatibility with SDC and LSGM electrolytes, respectively. However, the long-term stability of LnBCO–SDC and LnBCO–LSGM composites need to be further investigated.

3.2. Electrical conductivity

Fig. 4 shows the variation of electrical conductivity with the temperature for LnBCO samples in air. The conductivity of all the LnBCO samples decreases as the measuring temperature is increased, which exhibits a metallic-like conduction behavior. For example, the conductivity value of PrBCO sample, which is 1343 S cm^{-1} at 300 °C, decreases rapidly to 618 S cm^{-1} at 850 °C. The faster decrease of conductivity at higher temperatures is closely related to the formation of significant amount of oxide vacancies. The formation of oxide vacancies is accompanied by a reduction of Co^{4+} to Co^{3+}, thus results in a decrease of the charge carrier concentration and Co–O covalency, and hence the electrical conductivity at higher temperatures. Also, the oxide vacancies will perturb the O–Co–O periodic potential, results in carrier localization [32], thus decreasing the electrical conductivity in LnBCO samples at higher temperatures. In addition, as shown in Fig. 4, the conductivity of all the LnBCO samples follows the sequence: PrBCO > NdBCO > SmBCO > GdBCO in the temperature range studied. The decrease in conductivity with decreasing Ln^{3+} ion radii can be explained by the reduction of the orbital overlap. That is, the decreasing size of the Ln^{3+} ions from Ln = Pr to Gd will cause an increasing bending of the O–Co–O bonds. The increasing bending can narrow the bandwidth due to a decrease in the overlap between the O: 2*p* and Co: 3*d* orbitals. Meanwhile, the decreasing size of the Ln^{3+} ions also results in the decreasing covalency of the Co–O bonds and the increasing electron localization from Ln = Pr to Gd, and consequently causes the decrease of electrical conductivity [32–34]. The lowest electrical conductivity value of all the samples is still higher than 300 S cm^{-1} in air from 300 °C to 850 °C. This means that LnBCO samples could fulfill the requirements in electrical properties for use as IT-SOFC cathodes.

3.3. Thermal expansion behavior

Figs. 5 and 6 show the thermal expansion curves of the samples LnBCO and LnBCO–SDC in the temperature range 30–1000 °C in air, respectively. Similar to other Co-containing simple per-

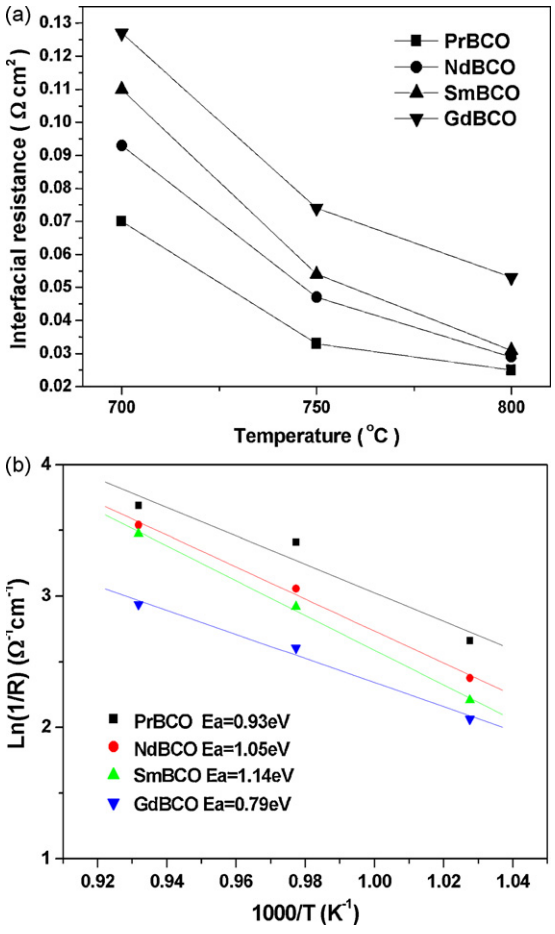

Fig. 7. (a) ASRs of LnBCO cathodes on LSGM electrolyte in symmetrical cells measured at 700–800 °C in air and (b) Arrhenius plots of the ASR values for LnBCO cathodes.

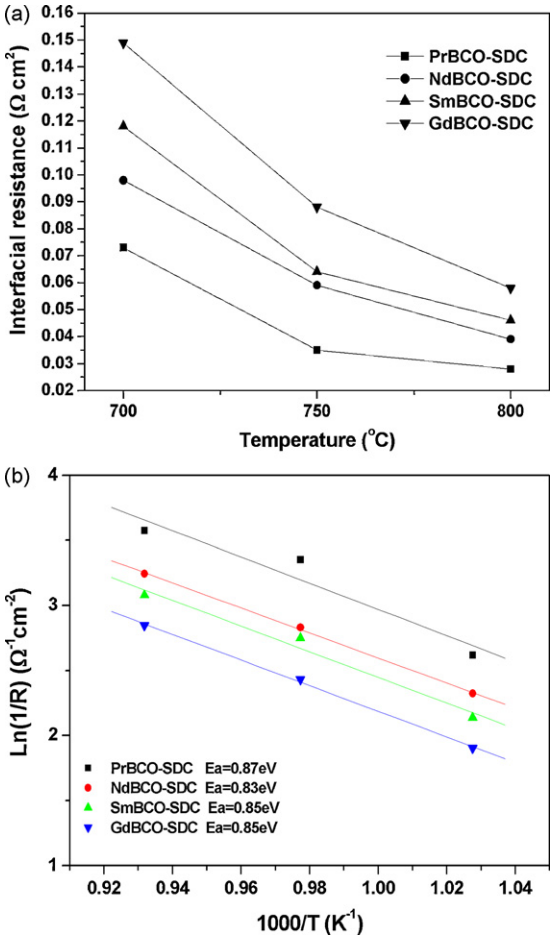

Fig. 8. (a) ASRs of LBCO–SDC composite cathodes on LSGM electrolyte in symmetrical cells measured at 700–800 °C in air and (b) Arrhenius plots of the ASR values for LnBCO–SDC composite cathodes.

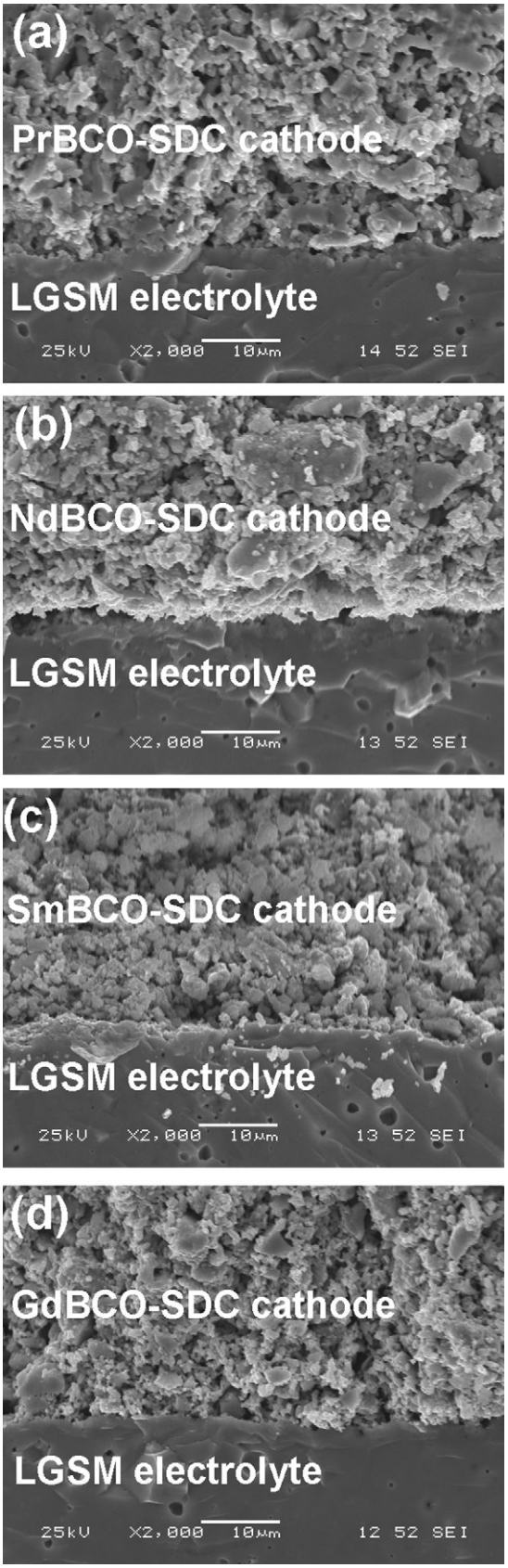

Fig. 9. SEM micrographs of the cross-sections of the cathode/electrolyte interface after the cell testing: (a) PrBCO–SDC/LSGM; (b) NdBCO–SDC/LSGM; (c) SmBCO–SDC/LSGM; and (d) GdBCO–SDC/LSGM. The composite cathodes on LSGM electrolyte were sintered at 950 °C for 2 h in air.

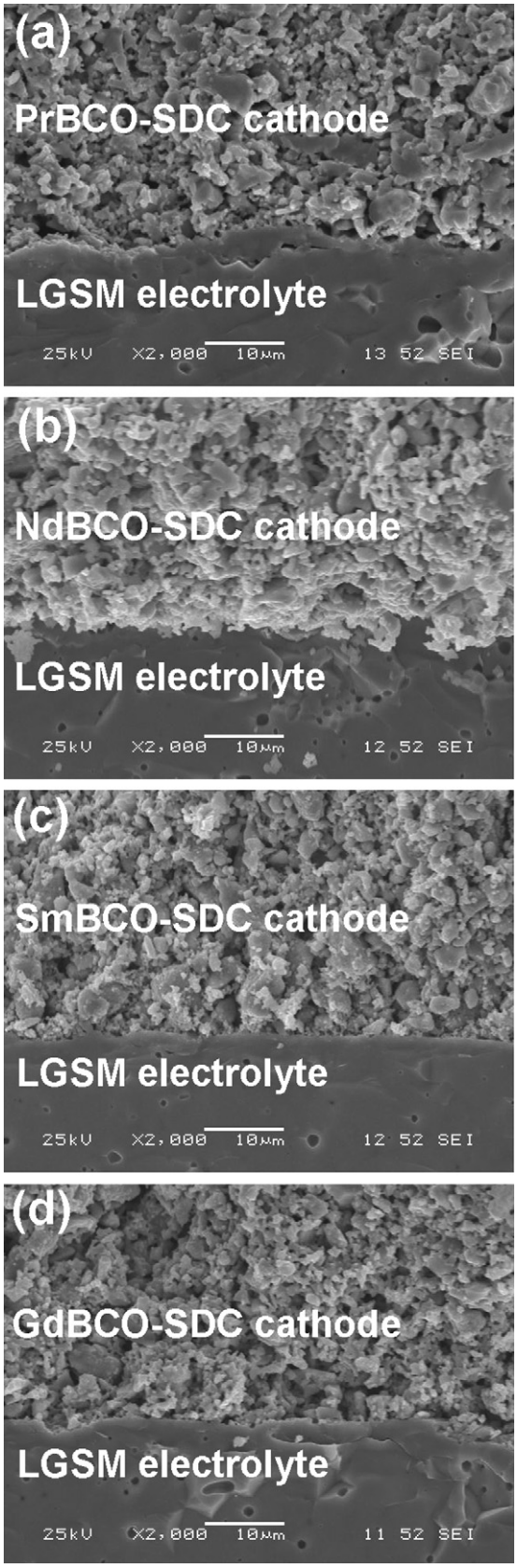

Fig. 10. SEM micrographs of the cross-sections of the cathode/electrolyte interface after the cell testing at 700 °C for 20 h: (a) PrBCO–SDC/LSGM; (b) NdBCO–SDC/LSGM; (c) SmBCO–SDC/LSGM; and (d) GdBCO–SDC/LSGM.

voskite oxides, the thermal expansion coefficient of LnBCO oxides is extraordinarily high. The TEC values of LnBCO oxides decreased from $21.5 \times 10^{-6}\,K^{-1}$ to $17.6 \times 10^{-6}\,K^{-1}$ with the change from Ln = Pr to Gd in the temperature range 30–1000 °C in air. The downtrend of TECs in LnBCO oxides from Ln = Pr to Gd is in good agreement with the results reported by Kim and Manthiram [8]. The TEC of samples is strongly related to the crystal structure. Generally, the TEC is smaller for the smaller unit cell of the same crystal structure, since the binding energy between ions in the lattice becomes large with the decrease in ionic distance [35]. We can see that the cell volume of LnBCO oxides decreases gradually with the decrease of Ln^{3+} ionic radii [8,11,14,19]. For example, the cell volume reduces from 116.30 Å^3 for PrBCO to 114.15 Å for GdBCO [14], thus resulting in a decrease of TEC in LnBCO oxides from Ln = Pr to Gd. In addition, the TEC decrease in LnBCO oxides is also due to the decrease in the ionicity of the Ln–O bonds as the ionic bonds generally reveal larger thermal expansion than covalent bonds [8]. As expected, the introduction of SDC into LnBCO efficiently reduced the TECs of the composite cathodes. For PrBCO cathode, the TEC of $21.5 \times 10^{-6}\,K^{-1}$ decreased to $20.1 \times 10^{-6}\,K^{-1}$ for PrBCO–SDC composite cathodes. The TEC decreased from $17.6 \times 10^{-6}\,K^{-1}$ for GdBCO cathode to $16.7 \times 10^{-6}\,K^{-1}$ for its composite cathode. The reduction of the TEC of composite cathodes is mainly attributed to the smaller TEC of SDC, for example, the TEC of SDC is $12.3 \times 10^{-6}\,K^{-1}$ in the temperature range of 350–900 °C in air [36].

3.4. Area specific resistance (ASR)

The ASRs of LnBCO cathodes and LnBCO–SDC composite cathodes on LSGM electrolyte measured at various temperatures in air are shown in Figs. 7(a) and 8(a). The impedance data were obtained using a symmetrical cell arrangement [10], and the cathode ASR is defined as follow: ASR = (resistance of electrode × area of electrode)/2. As expected, the increase of the measurement temperature results in a significant reduction of the ASRs. We can see from Figs. 7(a) and 8(a) that the ASRs of LnBCO–SDC composite cathodes are similar to those of LnBCO cathodes. However, the values of ASRs of LnBCO–SDC composite cathodes are slightly higher than those of LnBCO cathodes on LSGM electrolyte at the same temperature, meaning that the introduction of SDC does not improve the electrochemical performance of the LnBCO cathodes. This result can be interpreted as follows. Partially, the reason is due to the oxygen-ion conductivity of LnBCO is a little higher than that of SDC. For example, Taskin et al. [37,38] reported that the oxygen ionic conductivity of $GdBaCo_2O_{5+x}$ was as high as $0.01\,S\,cm^{-1}$ at 500 °C, while the oxygen ionic conductivity of SDC was reported by others as $1.2 \times 10^{-2}\,S\,cm^{-1}$ [39] and $5 \times 10^{-3}\,S\,cm^{-1}$ [40] at 600 °C. The lower oxygen ionic conductivity of LnBCO–SDC composites reduces the intrinsic rapid oxygen-ion diffusion and surface exchange kinetics of LnBCO oxides, and this lowers in turn the catalytic activity [5,6,37,41], thus leading to an increased ASR of LnBCO–SDC composite cathodes. More importantly, the electronic

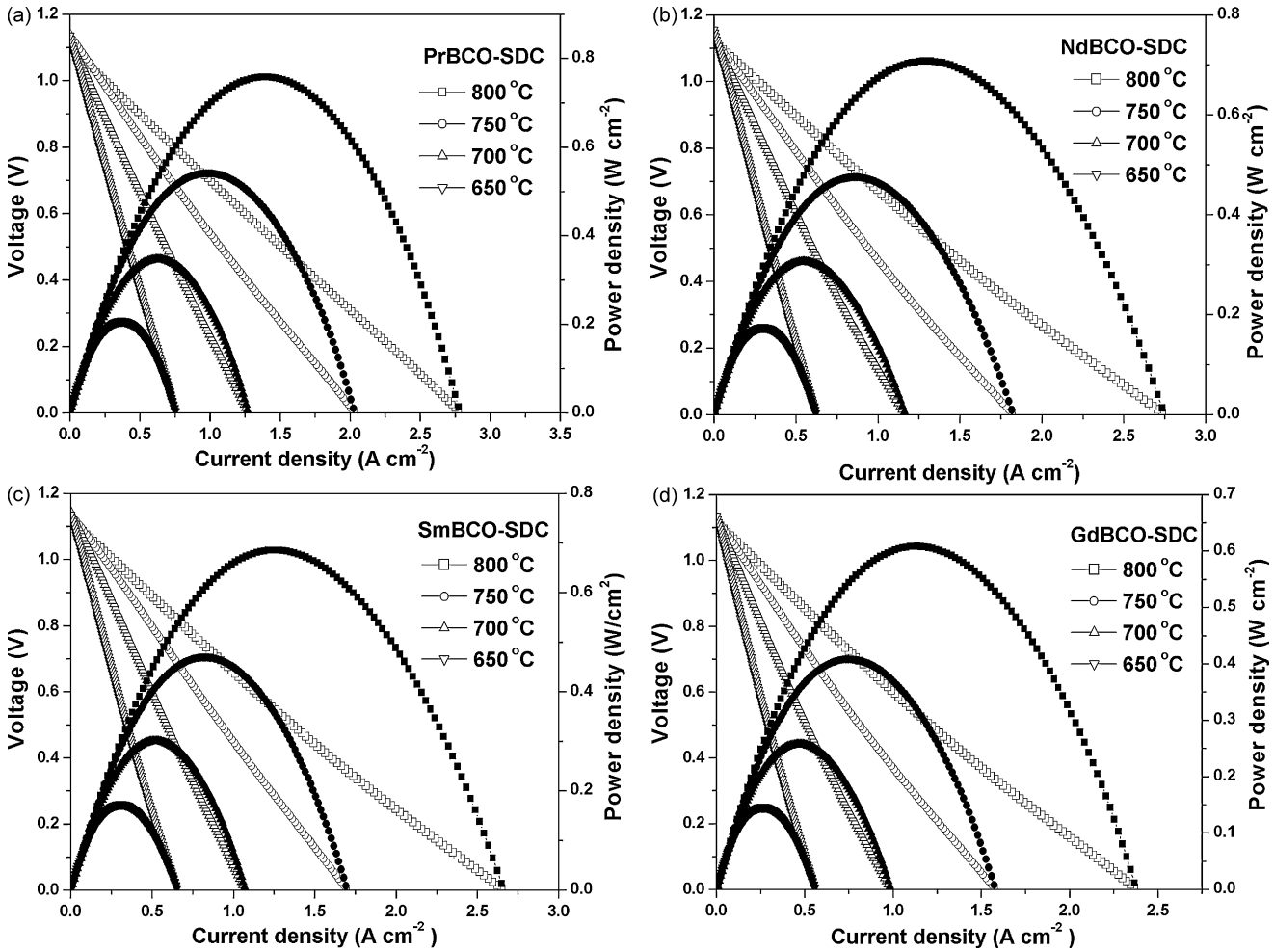

Fig. 11. Power density and voltage as a function of current density for cell LnBCO–SDC/LSGM/SDC/Ni–SDC using H_2 as fuel and ambient air as oxidant in the temperature range of 650–800 °C.

conductivity of LnBCO oxides is significantly higher than that of SDC. So the introduction of SDC into LnBCO decreases the electrical conductivity of LnBCO–SDC composite cathodes, thus causing an inferior current collection and process of charge transfer for the whole cathode, and hence the increased ASR of composite cathodes. In addition, we can see from Figs. 7(a) and 8(a) that the ASRs of LnBCO cathodes and LnBCO–SDC composite cathodes increase as size of the Ln^{3+} ions decreases from Ln = Pr to Gd. This is because the LnBCO bulk diffusion coefficient and surface exchange coefficient decreases with decreasing size of the Ln^{3+} ions from Pr to Gd [4,11,38]. The ASR values of the LnBCO cathodes are 0.070 $\Omega\,cm^2$, 0.093 $\Omega\,cm^2$, 0.110 $\Omega\,cm^2$ and 0.127 $\Omega\,cm^2$ at 700 °C with the shift from Ln = Pr to Gd, respectively, while LnBCO–SDC composite cathodes are 0.073 $\Omega\,cm^2$, 0.098 $\Omega\,cm^2$, 0.118 $\Omega\,cm^2$ and 0.149 $\Omega\,cm^2$ at the same temperature, respectively. The ASR values are all lower than 0.15 $\Omega\,cm^2$ at 700 °C, an expected criterion for the ASR of the cathode [42]. These results demonstrate that LnBCO and LnBCO–SDC oxides are very suitable cathode materials for IT-SOFCs.

Figs. 7(b) and 8(b) show Arrhenius plots of the ASR values for LnBCO cathodes and LnBCO–SDC composite cathodes, respectively. The specific data for the activation energy are also shown in Figs. 7(b) and 8(b), respectively. The activation energy of the composite cathodes decreases compared to LnBCO cathodes, although there are some small deviations. This is mainly because the addition of the SDC electrolyte effectively extends electrochemical triple-phase boundary and increases the number of active sites, thus decreasing the activation energy of the composite cathodes. A similar result has been recently reported in the $SmBaCo_2O_{5+d}$ (SmBCO) and $Ce_{0.9}Gd_{0.1}O_{2-d}$ (CGO91) composite cathodes, which the activation energies decreased with CGO91 content [43].

To assess the thermal compatibility and the long-term thermal stability of the cathode/electrolyte interface, SEM was used to observe the cross-section of the cathode/electrolyte interface of the cell. Figs. 9 and 10 are the SEM micrographs of the cross-sections of the cathode/electrolyte interface after the cell testing and testing at 700 °C for 20 h, respectively. As can be seen from Figs. 9 and 10, a good bonding and continuous contact at the cathode/electrolyte interface is retained after the cell testing and testing at 700 °C for 20 h, respectively. No delamination of the cathode from the electrolyte is observed in the SEM micrographs, indicating the good thermal compatibility between the two materials and the thermal stability of the cathode/electrolyte interface. These results are in full agreement with the assertion of Kim and Manthiram [8], who stated that the $LnBaCo_2O_{5+x}$ cathodes with an intermediate lanthanide-ion radius such as Ln = Nd, Sm, and Gd was preferred, in view of the trade-off between the values of the catalytic activity and TEC.

In addition, the TEC of the LnBCO–SDC composite cathodes can be further reduced with increasing electrolyte content. For example, Kim et al. [43] recently reported that the TEC of the SmBCO–CGO91 composite cathode, was reduced from $20.2 \times 10^{-6}\,K^{-1}$ for pure SmBCO to $13.3 \times 10^{-6}\,K^{-1}$ for 50 wt% SmBCO–50 wt% CGO91, which was very close to the value of the CGO91 electrolyte.

3.5. Single-cell performance

Fig. 11 shows power density and voltage as a function of current density for cells LnBCO–SDC/LSGM/SDC/Ni-SDC using H_2 as fuel and ambient air as oxidant at different temperatures. It can be seen from Fig. 11, the power density of single-cell for LnBCO–SDC composite cathodes decreases as size of the Ln^{3+} ions is decreased from Ln = Pr to Gd. This result is in good agreement with the results of electrical conductivity and ASR (see Figs. 4, 7 and 8) discussed above. At 800 °C, the maximum power density of cell using LnBCO–SDC composite cathodes is 758, 707, 685 and 608 mW cm^{-2} with the change from Ln = Pr to Gd, respectively. Thus, the relatively higher power densities indicate the better electrochemical performances of the LnBCO–SDC composite cathodes for IT-SOFCs. These results again demonstrate that the rapid oxygen-ion diffusion and surface exchange kinetics of LnBCO oxide may play dominant roles in the electrochemical performance of cells [8,38].

4. Conclusions

The single phase double-perovskite oxides LnBCO were prepared with a solid-state reaction. The performances of LnBCO–SDC oxides were examined as composite cathodes for IT-SOFCs. The conductivity of samples LnBCO obeyed in the following order: PrBCO > NdBCO > SmBCO > GdBCO in the temperature range studied, and the lowest conductivity was higher than 300 S cm^{-1}. The introduction of SDC into LnBCO efficiently reduced the TECs of the composite cathodes. The electrochemical performances of LnBCO and LnBCO–SDC cathodes decreased as size of the Ln^{3+} ions was decreased from Ln = Pr to Gd. The ASRs of the LnBCO cathodes and LnBCO–SDC composite cathodes were lower than 0.13 $\Omega\,cm^2$ and 0.15 $\Omega\,cm^2$ at 700 °C, respectively. The maximum power density of single-cell with LnBCO–SDC composite cathodes decreased from 758 mW cm^{-2} to 608 mW cm^{-2} at 800 °C with the change from Ln = Pr to Gd, respectively. These results demonstrated that LBCO–SDC composite cathodes were a promising cathode material for IT-SOFCs. The introduction of SDC into LnBCO to make a composite cathode decreased the electrochemical performances of LnBCO cathodes slightly. This indicated that the intrinsic rapid oxygen-ion diffusion and surface exchange kinetics of LnBCO oxides played dominant roles in the electrochemical performance of cells.

Acknowledgement

This work was supported by the Natural Science Foundation of China under contract No. 10974065.

References

[1] B.C.H. Steele, A. Heinzel, Nature 414 (2001) 345–352.
[2] S.J. Skinner, Int. J. Inorg. Mater. 3 (2001) 113–121.
[3] A.M. Chang, S.J. Skinner, J.A. Kilner, Solid State Ionics 177 (2006) 2009–2011.
[4] G. Kim, S. Wang, A.J. Jacobson, L. Reimus, P. Brodersen, C.A. Mims, J. Mater. Chem. 17 (2007) 2500–2505.
[5] A. Tarancón, S.J. Skinner, R.J. Chater, F. Hernández-Ramírez, J.A. Kilner, J. Mater. Chem. 17 (2007) 3175–3181.
[6] A. Tarancón, A. Morata, G. Dezanneau, S.J. Skinner, J.A. Kilner, S. Estradé, F. Hernández-Ramírez, F. Peiró, J.R. Morante, J. Power Sources 174 (2007) 255–263.
[7] N. Li, Z. Lü, B. Wei, X.Q. Huang, K.F. Chen, Y.H. Zhang, W.H. Su, J. Alloy Compd. 454 (2008) 274–279.
[8] J.-H. Kim, A. Manthiram, J. Electrochem. Soc. 155 (4) (2008) B385–390.
[9] B. Lin, S. Zhang, L. Zhang, L. Bi, H. Ding, X. Liu, J. Gao, G. Meng, J. Power Sources 177 (2008) 330–333.
[10] Q. Zhou, T. He, Y. Ji, J. Power Sources 185 (2008) 754–758.
[11] K. Zhang, L. Ge, R. Ran, Z. Shao, S. Liu, Acta Mater. 56 (2008) 4876–4889.
[12] E. Chavez, M. Mueller, L. Mogni1, A. Caneiro, J. Phys.: Conf. Ser. 167 (2009), 012043-1-6.
[13] C. Martin, A. Maignan, D. Pelloquin, N. Nguyen, B. Raveau, Appl. Phys. Lett. 71 (1997) 1421–1423.
[14] A. Maignan, C. Martin, D. Pelloquin, N. Nguyen, B. Raveau, J. Solid State Chem. 142 (1999) 247–260.
[15] F. Fauth, E. Suard, V. Caignaert, B. Domengès, I. Mirebeau, L. Keller, Eur. Phys. J. B21 (2001) 163–174.
[16] A.A. Taskin, A.N. Lavrov, Y. Ando, Phys. Rev. B 71 (2005), 134414-1-28.
[17] M. Respaud, C. Frontera, J.L. García-Muñoz, M.A.G. Aranda, B. Raquet, J.M. Broto, H. Rakoto, M. Goiran, A. Llobet, J. Rodríguez-Carvajal, Phys. Rev. B 64 (2001), 214401-1-7.
[18] C. Frontera, J.L. Garcia-Munoz, A.E. Carrillo, C. Ritter, D.M. Marero, A. Caneiro, Phys. Rev. B 70 (2004), 184428-1-9.
[19] S. Roy, I.S. Dubenko, M. Khan, E.M. Condon, J. Craig, N. Ali, Phys. Rev. B 71 (2005), 024419-1-8.
[20] J.-E. Jørgensen, L. Keller, Phys. Rev. B 77 (2008), 024427-1-7.
[21] C. Zhu, X. Liu, C. Yi, D. Yan, W. Su, J. Power Sources 185 (2008) 193–196.
[22] D. Chen, R. Ran, K. Zhang, J. Wang, Z. Shao, J. Power Sources 188 (2009) 96–105.

[23] H. Gu, H. Chen, L. Gao, Y. Zheng, X. Zhu, L. Guo, Int. J. Hydrogen Energy 34 (2009) 2416–2420.
[24] B. Lin, Y. Dong, R. Yan, S. Zhang, M. Hu, Y. Zhou, G. Meng, J. Power Sources 186 (2009) 446–449.
[25] W. Sun, L. Bi, L. Yan, R. Peng, W. Liu, J. Alloy Compd. 481 (2009) L40–L42.
[26] A. Tarancón, J. Peña-Martínez, D. Marrero-López, A. Morata, J.C. Ruiz-Morales, P. Núñez, Solid State Ionics 179 (2008) 2372–2378.
[27] J. Peña-Martínez, A. Tarancón2, D. Marrero-López, J.C. Ruiz-Morales, P. Núñez, Fuel Cells 8 (5) (2008) 351–359.
[28] J.-H. Kim, F. Prado, A. Manthiram, J. Electrochem. Soc. 155 (10) (2008) B1023–B1028.
[29] Y. Liu, J. Alloys Compd. 477 (2009) 860–862.
[30] J.H. Kim, M. Cassidy, J.T.S. Irvine, J. Bae, J. Electrochem. Soc. 156 (6) (2009) B682–B689.
[31] L. Cong, T. He, Y. Ji, P. Guan, Y. Huang, W. Su, J. Alloy Compd. 348 (2003) 325–331.
[32] H. Takahashi, F. Munakata, M. Yamanaka, Phys. Rev. B 57 (1998) 15211–15218.
[33] S. Yamaguchi, Y. Okimoto, Y. Tokura, Phys. Rev. B 54 (1996) R11022–R11025.
[34] K.T. Lee, A. Manthiram, J. Electrochem. Soc. 153 (4) (2006) A794–A798.
[35] H. Hayashi, M. Watanabe, M. Ohuchida, H. Inaba, Y. Hiei, T. Yamamoto, M. Mori, Solid State Ionics 144 (2001) 301–313.
[36] E.Y. Pikalova, V.I. Maragou, A.N. Demina, A.K. Demin, P.E. Tsiakara, J. Power Sources 181 (2008) 199–206.
[37] A.A. Taskin, A.N. Lavrov, Y. Ando, Appl. Phys. Lett. 86 (2005), 091910-1-3.
[38] A.A. Taskin, A.N. Lavrov, Y. Ando, Prog. Solid State Chem. 35 (2007) 481–490.
[39] G.B. Balazs, R.S. Glass, Solid State Ionics 76 (1995) 155–162.
[40] W. Huang, P. Shuk, M. Greenblatt, Solid State Ionics 100 (1997) 23–27.
[41] G. Kim, S. Wang, A.J. Jacobson, Appl. Phys. Lett. 88 (2006), 024103-1-3.
[42] B.C.H. Steele, Solid State Ionics 86–88 (1996) 1223–1234.
[43] J.H. Kim, Y. Kim, P.A. Connor, J.T.S. Irvine, J. Baea, W. Zhou, J. Power Sources 194 (2009) 704–711.